Research Article

S. Ravikumar, Maimona Rafiq*, Dilsora Abduvalieva, and Fuad A. Awwad

Effects of Joule heating and reaction mechanisms on couple stress fluid flow with peristalsis in the presence of a porous material through an inclined channel

https://doi.org/10.1515/phys-2023-0118
received August 01, 2023; accepted September 24, 2023

Abstract: The objective of this study is to assess the flow behavior of the peristalsis mechanism of a couple stress fluid in incorporating a porous material. In addition, reaction mechanism and Ohmic heating are also taken into consideration with slip boundary conditions. For the purposes of mathematical simulation, we assume a long-wavelength approximation, ignoring the wave number and taking a low Reynolds number into account. The obtained outcome is shown in a graphical manner and then analyzed. The results of this investigation reveal that when the Hartmann number improves, the pattern of velocity noticeably decelerates. The Lorentz forces have a retarding impact on the velocity of the fluid from a physical standpoint. As the couple stress variable rises, so does the velocity of the fluid. As the couple stress component increases, the skin friction coefficient increases in one region of the fluid channel and falls in another region, between x = 0.5 and x = 1. As the thermal slip variable rises, more heat is transferred through the surface to the fluid, resulting in a rise in the temperature profile. When the couple stress variable is raised, the Nusselt number rises, while the thermal radiation factor causes the Nusselt number to decline. The results showed a positive relationship between the Sherwood number and the reaction mechanism parameter. This study demonstrates the potential use of this research in the fields of a career in engineering, namely, in enhancing hydraulic systems, as well as in medicine, particularly in optimizing gastrointestinal processes. The process of dissection facilitates the unimpeded circulation of blood and lymph inside the vascular system of the body, enabling the delivery of oxygen to tissues and the elimination of waste materials.

Keywords: heat transfer, porous material, chemical reaction, incline channel, joule heating, and mass transfer

Nomenclature

$\bar{u}$	velocity along $\bar{x}$ direction
$\bar{v}$	velocity along $\bar{y}$ direction
p	pressure gradient
d	channel width (m)
a	wave amplitude (m)
λ	wavelength
μ	viscosity of the fluid (kg/m/s)
σ	electrical conductivity of the fluid
c	wave speed (m/s)
C_p	specific heat at constant pressure
ρ	density of the fluid (kg/m^3)
T	temperature of the fluid
k	thermal conductivity
k_1	porous medium permeability
β	heat source/sink
Re	Reynolds number
M	Hartmann number
Da	porosity parameter
m	Hall current parameter
ϕ	amplitude ratio
δ	wave number

*** Corresponding author: Maimona Rafiq**, Department of Mathematics, COMSATS University Islamabad, Attock, 43600, Pakistan, e-mail: maimona_88@hotmail.com
S. Ravikumar: Department of Mathematics, NBKR Institute of Science and Technology (Autonomous), Vidyanagar, Tirupati district, Andhra Pradesh, Pin-524413, India; School of Electronics, College of Engineering, Peking University, Peking, 100871, China, e-mail: drsravikumar1979@gmail.com
Dilsora Abduvalieva: Tashkent State Pedagogical University, Bunyodkor Avenue, 27, Tashkent, 100070, Uzbekistan, e-mail: editory1001@gmail.com
Fuad A. Awwad: Department of Quantitative Analysis, College of Business Administration, King Saud University, P.O. Box 71115, Riyadh, 11587, Saudi Arabia, e-mail: fawwad@ksu.edu.sa

Ω	rotation parameter
Br	Brinkman number
Rn	thermal radiation parameter (W m^2/K)
Pr	Prandtl number
θ	temperature distribution
Sr	Soret number
Sc	Schmidt number
S	chemical reaction parameter
η_1, η_2	gravitational parameters

1 Introduction

Couple stress fluids are a subclass of non-Newtonian fluids characterized by their consideration of the size of fluid particles. Since fluids displaying couple stress have so many practical and theoretical consequences, their study has attracted a lot of attention from scholars. The couple stress fluid concept may also be applied to understand the dynamics of blood flow inside arterial arteries. Numerous scholars have conducted investigations on the behavior of pair stress fluids in the framework of peristaltic mechanism difficulties under various conditions. Eldabe *et al.* [1] investigated the role of wall features on the physiological behavior of a couple stress fluid. Abou-zeid and Mohamed [2] did research using the perturbation method to examine the physiological fluid mechanism of a couple stress fluid during magnetohydrodynamic (MHD) circumstances. Alsaedi *et al.* [3] explored the physiological transport across a homogeneously porous substrate. Researchers [4–14] have used computational techniques to examine couple stress fluid flow with peristalsis in a wide range of contexts.

The peristaltic process has gained popularity in recent decades. The fields of medicine and physiology have found several uses for peristalsis. Some examples of gastrointestinal motility include sperm traveling through the coronary arteries, lymphatic fluid traveling through lymph veins, blood cells migrating through the vasculature, and organs being shifted about in the abdomen. Theoretical and experimental discussions of the peristalsis of viscous fluids may be found in the works of Latham [15] and Shapiro *et al.* [16]. Numerous studies [17–26] looked at peristaltic flow under the low Reynolds number assumptions of the long-wavelength approximation. Furthermore, in recent years, researchers focusing on geo-substantial solution dynamics have shown a marked uptick in interest in exploring fluid flow models within porous materials. The study carried out by Ramesh Babu *et al.* [27] looked at the phenomenon of the physiological mechanism of a viscous fluid across a porous substance using the lubrication concept technique. Aman *et al.* [28] studied how Maxwell fractional fluid through porous material affects heat transmission. Heat and mass transfer are major concerns for MHD fluxes. According to Hayat *et al.* [29], the convective heat transmission capabilities of Carreau fluid are due to the Joule heating caused by the MHD peristalsis of the fluid. Non-Newtonian fluids' mixed convective peristaltic transport was investigated by Abbasi *et al.* [30], who looked at how Ohmic heating affected it. According to Hayat *et al.* [31], a radiation-heated magneto nanofluid flowing through a porous material exhibits a peristaltic motion. The peristaltic mechanism was studied for its role in heat and mass transfer by Prasad *et al.* [32]. The study of heat and mass transfer in fluid systems, in conjunction with chemical processes, has gained significance in the fields of metallurgy and chemical engineering. Bestman [33] was the first to investigate chemical reactions in interface-layer streams. Reddy *et al.* [34] explored the impact of radiation on the expansion of a linearly expanding sheet carrying a chemically reacting Maxwell fluid *via* a MHD field. Numerous researchers have recently looked at how chemical reactions influence the fluid flow patterns seen on different surfaces [35 –39].

The peristaltic flows of non-Newtonian fluids are the focus of all the aforementioned works. Several of these works also discussed the impacts of reaction mechanism, Joule heating, radiation, and couple stress. The major focus of this work is on studying the peristaltic couple stress fluid under temperature and concentration slip conditions along the rotating effects. Our study may be helpful in directing future research in this area since, to the best of our knowledge, this kind of analytical model has never been explored in any published work previously. Heat and mass transport with Ohmic heating and chemical reaction in an asymmetric channel may be analyzed using a couple stress fluid with a peristaltic mechanism ([9] and [40]) and fluid flow and different techniques. Physical interpretation of penetration energy absorption energy of 2A12 aluminum alloy, relaxation of Epoxy resin on dielectric loss of medium-frequency transformer, and characteristics of centrifugal pump are highlighted in previously published studies [41–43]. Numerous works [44–46] depicted the applications of porous nanosheets for highly efficient photocatalytic degradation of refractory contaminants, coupled thermo-hydro-mechanical mechanism, and colloidal suspension transport in porous media. Previous studies [47–50] highlighted some recent developments in fluid flow *versus* various flow assumptions. Sun *et al.* [51] and Xiang *et al.* [52] recently worked on shear-thickening fluids and micro-fluidic chip structured with micro-wedge array.

The novel aspects of this study make it exceptional. Due to its significance in public health applications, thermal radiation has gained substantial importance in the area of medical research. Several skin conditions have been successfully treated using infrared radiation techniques in dermatology. These techniques may also promote better blood flow to certain bones by acting as a kind of thermotherapy. Previous studies [53–57] highlighted some recent advancements in the field of fluid dynamics subject to different geometries.

The following questions are at the heart of the study that inspired this article:

- How does the couple stress component affect the fluid velocity and the skin friction coefficient?
- How do the thermal slip parameter, thermal radiation, and couple stress parameter affect heat transfer?
- How do reaction constant, concentration slip parameter, and Soret number influence mass transfer?
- How are the Nusselt number (Nu) and Sherwood number (Sh) at the wall $y = h$ influenced by different parameters?

2 Formulation of the model

Consider the physiological mechanism of a couple stress incompressible, viscous fluid over a uniform thickness in the occurrence of an external magnetic field. Furthermore, the consideration of heat and mass transfer under slip circumstances is included. The fluid is stimulated by sinusoidal wave trains moving along the channel walls at a constant speed c. Figure 1 depicts the physical model of the problem and the flow coordinate system [9].

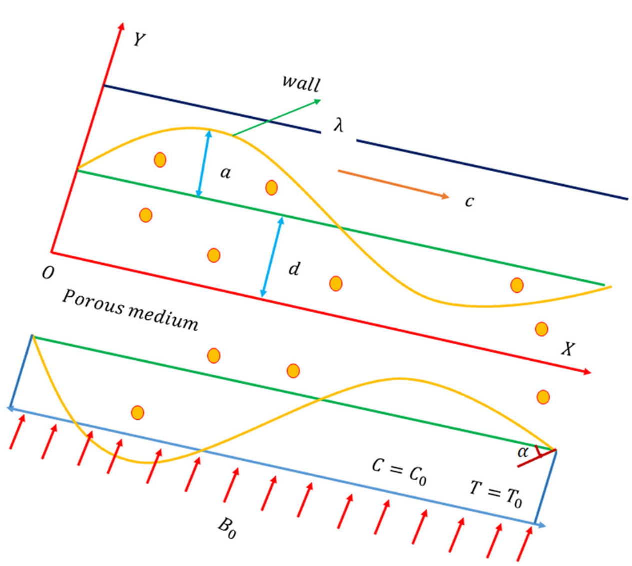

Figure 1: Physical model illustration.

$$\bar{Y} = \bar{H} = d + a\sin\left[\frac{2\pi}{\lambda}(\bar{X} - c\bar{t})\right], \tag{1}$$

where a, t, d, and λ are the wave amplitude, time, half-width of the channel, and wavelength.

In a wave reference system, the governing equations are given by [58]:

$$\frac{\partial\bar{u}}{\partial\bar{x}} + \frac{\partial\bar{v}}{\partial\bar{y}} = 0, \tag{2}$$

$$\begin{aligned}\rho\left[\bar{u}\frac{\partial\bar{u}}{\partial\bar{x}} + \bar{v}\frac{\partial\bar{u}}{\partial\bar{y}}\right] - \rho\left(\Omega^2\bar{u} + 2\Omega\frac{\partial\bar{v}}{\partial\bar{t}}\right) &= -\frac{\partial\bar{p}}{\partial\bar{x}} + \mu\left[\frac{\partial^2\bar{u}}{\partial\bar{x}^2} + \frac{\partial^2\bar{u}}{\partial\bar{y}^2}\right] - \eta\left[\frac{\partial^4\bar{u}}{\partial\bar{x}^4} + \frac{\partial^4\bar{u}}{\partial\bar{y}^4}\right.\\ &\left. + 2\frac{\partial^4\bar{u}}{\partial\bar{x}^2\partial\bar{y}^2}\right] - [\sigma B_0{}^2](\bar{u} + c) - \left[\frac{\mu}{k_1}\right](\bar{u} + c)\\ &+ \rho g\sin\gamma,\end{aligned} \tag{3}$$

$$\begin{aligned}\rho\left[\bar{u}\frac{\partial\bar{v}}{\partial\bar{x}} + \bar{v}\frac{\partial\bar{v}}{\partial\bar{y}}\right] + \rho\left(-\Omega^2\bar{v} + 2\Omega\frac{\partial\bar{u}}{\partial\bar{t}}\right) &= -\frac{\partial\bar{p}}{\partial\bar{y}} + \mu\left[\frac{\partial^2\bar{v}}{\partial\bar{x}^2} + \frac{\partial^2\bar{v}}{\partial\bar{y}^2}\right] - \eta\left[\frac{\partial^4\bar{v}}{\partial\bar{x}^4} + \frac{\partial^4\bar{v}}{\partial\bar{y}^4}\right.\\ &\left. + 2\frac{\partial^4\bar{v}}{\partial\bar{x}^2\partial\bar{y}^2}\right] - \rho g\cos\gamma,\end{aligned} \tag{4}$$

$$\rho C_p\left[\bar{u}\frac{\partial\bar{T}}{\partial\bar{x}} + \bar{v}\frac{\partial\bar{T}}{\partial\bar{y}}\right] = k\left[\frac{\partial^2\bar{T}}{\partial\bar{x}^2} + \frac{\partial^2\bar{T}}{\partial\bar{y}^2}\right] + Q_0 + \sigma B_0^2\bar{u}^2 - \frac{\partial\bar{q}_r}{\partial\bar{y}}, \tag{5}$$

$$\left[\bar{u}\frac{\partial\bar{C}}{\partial\bar{x}} + \bar{v}\frac{\partial\bar{C}}{\partial\bar{y}}\right] = D_m\left[\frac{\partial^2\bar{C}}{\partial\bar{x}^2} + \frac{\partial^2\bar{C}}{\partial\bar{y}^2}\right] + \frac{D_m K_T}{T_m}\left[\frac{\partial^2\bar{T}}{\partial\bar{x}^2} + \frac{\partial^2\bar{T}}{\partial\bar{y}^2}\right] - k_2(\bar{C} - C_0)\,. \tag{6}$$

For thermal radiation, using the Rosseland approximation [59,60], we have

$$\bar{q}_r = \frac{16\sigma^* T_0{}^3}{3k^*}\frac{\partial T}{\partial y}. \tag{7}$$

The transformation allows us to extend the fixed (X,Y) frame with a wave frame (x,y) that travels away from it at c:

$$\bar{y} = \bar{Y},\ \text{and}\ \bar{x} = \bar{X} - c\bar{t}. \tag{8}$$

Non-dimensional measures [58]:

$$\left.\begin{aligned}
&\bar{x} = \frac{x}{\lambda}, \; \bar{y} = \frac{y}{d}, \; \bar{t} = \frac{ct}{\lambda}, \; \bar{u} = \frac{u}{c}, \; \bar{v} = \frac{v}{c\delta}, \; \bar{p} = \frac{d^2 p}{c\lambda\mu},\\
&\varepsilon = \frac{a}{d}, \; \delta = \frac{d}{\lambda},\\
&\mathrm{Da} = \frac{k_1}{d^2}, \mathrm{Re} = \frac{\rho c d}{\mu}, \; M = B_0 d\sqrt{\frac{\sigma}{\mu}}, \; \mathrm{Pr} = \frac{\mu C_p}{\kappa},\\
&\beta = \frac{Q_0 d^2}{\mu C_p (T_1 - T_0)},\\
&\theta = \frac{\bar{T} - T_0}{T_1 - T_0}, \; \propto = \sqrt{\frac{\mu}{\eta}} d, \Phi = \frac{\bar{C} - C_0}{C_1 - C_0}, \; \eta_1 = \frac{\rho d^2 g}{\mu c},\\
&\eta_2 = \frac{\rho d^3 g}{\lambda \mu c}, \; \mathrm{Sc} = \frac{\mu}{D_m \rho},\\
&\mathrm{Sr} = \frac{D_m \rho \, k_T (T_1 - T_0)}{\mu T_m (C_1 - C_0)}, \; \mathrm{Rn} = \frac{16\sigma^* T_0^3 d^2}{3k^* \mu \, C_p}, \; S = \frac{K_2 \rho a^2}{\mu},
\end{aligned}\right\} \tag{9}$$

where ε, k_1, δ, Re, M, Da, α, η_1, η_2, Sr, S, ScPr, β are the amplitude ratio, non-uniform parameter, wave number, Reynolds number, Hartman number, porosity parameter, couple stress parameter, gravitational parameters, Soret number, chemical reaction parameter, Schmidt number, Prandtl number, heat source/sink parameter, and thermal radiation.

3 Solution of the problem

Dropping the bars from Eqs. (2)–(6) yields the following non-dimensional form when Eqs. (8) and (9) are implemented:

$$\delta\left[\frac{\partial u}{\partial x} + \frac{\partial u}{\partial y}\right] = 0, \tag{10}$$

$$\begin{aligned}
&\mathrm{Re}\delta\left[u\frac{\partial u}{\partial x} + v\frac{\partial u}{\partial y}\right] - \frac{\rho b^2 \Omega^2}{\mu} u - 2\,\mathrm{Re}\,\delta^2 \Omega \frac{\partial v}{\partial t} =\\
&-\frac{\partial p}{\partial x} + \delta^2 \frac{\partial^2 u}{\partial x^2} + \frac{\partial^2 u}{\partial y^2}\\
&-\frac{1}{\propto^2}\left(\delta^4 \frac{\partial^4 u}{\partial x^4} + \frac{\partial^4 u}{\partial y^4} + 2\delta^2 \frac{\partial^4 u}{\partial x^2 \partial y^2}\right)\\
&-\frac{\partial p}{\partial x} + \delta^2 \frac{\partial^2 u}{\partial x^2} + \frac{\partial^2 u}{\partial y^2}\\
&-\left(M^2 + \frac{1}{\mathrm{Da}}\right) u - \left(M^2 + \frac{1}{\mathrm{Da}}\right)\\
&+\eta_1 \sin\gamma,
\end{aligned} \tag{11}$$

$$\begin{aligned}
&\mathrm{Re}\delta^3\left[u\frac{\partial v}{\partial x} + v\frac{\partial v}{\partial y}\right] - \frac{\rho \Omega^2 b^2 \delta^2}{\mu} v + 2\,\mathrm{Re}\Omega\delta^2 \frac{\partial u}{\partial t} =\\
&-\frac{\partial p}{\partial y} + \delta^2\left(\delta^2 \frac{\partial^2 v}{\partial x^2} + \frac{\partial^2 v}{\partial y^2}\right)\\
&-\frac{1}{\propto^2}\delta^2\left(\delta^4 \frac{\partial^4 v}{\partial x^4} + \frac{\partial^4 v}{\partial y^4}\right.\\
&\left.+ 2\delta^2 \frac{\partial^4 v}{\partial x^2 \partial y^2}\right) - \eta_2 \cos\gamma,
\end{aligned} \tag{12}$$

$$\begin{aligned}
\mathrm{Re}\delta\left[u\frac{\partial \theta}{\partial x} + v\frac{\partial \theta}{\partial y}\right] = \frac{1}{\mathrm{Pr}}\left[\delta^2 \frac{\partial^2 \theta}{\partial x^2} + \frac{\partial^2 \theta}{\partial y^2}\right] + \beta + M^2 E_c u^2\\
+ \mathrm{Rn}\frac{\partial^2 \theta}{\partial y^2},
\end{aligned} \tag{13}$$

$$\begin{aligned}
\mathrm{Re}\delta\left[u\frac{\partial \phi}{\partial x} + v\frac{\partial \phi}{\partial y}\right] = \frac{1}{\mathrm{Sc}}\left[\delta^2 \frac{\partial^2 \phi}{\partial x^2} + \frac{\partial^2 \phi}{\partial y^2}\right]\\
+ \frac{1}{\mathrm{Sr}}\left[\delta^2 \frac{\partial^2 \phi}{\partial x^2} + \frac{\partial^2 \phi}{\partial y^2}\right]\\
- k_2 (C - C_0).
\end{aligned} \tag{14}$$

Eqs. (10)–(14) can be reduced to the following forms if we use the long-wavelength approximation and disregard the wave number, while taking into account low Reynolds scenarios [61]:

$$\frac{1}{\propto^2}\frac{\partial^4 u}{\partial y^4} - \frac{\partial^2 u}{\partial y^2} + f_1 u = -\frac{\partial p}{\partial x} - \left(M^2 + \frac{1}{\mathrm{Da}}\right) + \eta_1 \sin\gamma, \tag{15}$$

$$\frac{\partial p}{\partial y} = 0, \tag{16}$$

$$\frac{1}{\mathrm{Pr}}\frac{\partial^2 \theta}{\partial y^2} + \beta + M^2 E_c u^2 + \mathrm{Rn}\frac{\partial^2 \theta}{\partial y^2} = 0, \tag{17}$$

$$\frac{1}{\mathrm{Sc}}\frac{\partial^2 \phi}{\partial y^2} + \mathrm{Sr}\frac{\partial^2 \phi}{\partial y^2} - S\phi = 0. \tag{18}$$

Dimensionless boundary conditions

$$\frac{\partial u}{\partial y} = 0 \; \frac{\partial^3 u}{\partial y^3} = 0, \text{ at } y = 0, \tag{19}$$

$$u = 0, \; \frac{\partial^2 u}{\partial y^2} = 0 \text{ at } y = h, \tag{20}$$

$$\theta = 0, \; \Phi = 0 \text{ at } y = 0, \tag{21}$$

$$\theta + \beta_1 \frac{\partial \theta}{\partial y}, \; \Phi + \beta_2 \frac{\partial \Phi}{\partial y} \text{ at } y = h, \tag{22}$$

where $h = 1 + \epsilon \sin\{2\pi(x - t)\}$, and β_1 and β_2 are the thermal and concentration slip parameters, respectively.

Using the provided boundary conditions (19) and (20), Eq. (15) becomes

$$u(y) = f_3 \cosh[r_1 y] + f_4 \cosh[r_2 y] - f_2, \tag{23}$$

where

$$f_3 = \frac{f_2 - f_4 \cosh[r_2 h]}{\cosh[r_1 h]},\ f_4 = \frac{f_2 r_1^2}{(r_1^2 - r_2^2)\cosh[r_2 h]},$$

$$f_2 = \frac{1}{f_1}\left(\frac{dp}{dx} + M^2 + \frac{1}{\mathrm{Da}} - \eta_1 \sin\gamma\right),$$

$$r_1 = \sqrt{\frac{1 + \sqrt{1 - \left(\frac{4f_1}{\alpha^2}\right)}}{\left(\frac{2}{\alpha^2}\right)}},\ r_2 = \sqrt{\frac{1 - \sqrt{1 - \left(\frac{4f_1}{\alpha^2}\right)}}{\left(\frac{2}{\alpha^2}\right)}},$$

$$f_1 = \left(M^2 + \frac{1}{\mathrm{Da}} - \frac{\rho d^2 \Omega^2}{\mu}\right).$$

By applying boundary conditions (21) and (22) to the outcomes of Eqs. (17) and (18), we acquire

$$\begin{aligned}\theta(y) = {} & f_{23} + (f_5 - f_{13})\frac{y^2}{2} - 2f_7 \cosh[2r_1 y] \\ & - 2f_8 \cosh[2r_2 y] - 2f_9 \cosh[(r_1 + r_2)y] \\ & - 2f_{10}\cosh[(r_1 - r_2)y] - 2f_{11}\cosh[r_1 y] \\ & + 2f_{12}\cosh[r_2 y],\end{aligned} \tag{24}$$

where

$$f_5 = \left(\frac{-\mathrm{Pr}_\beta}{1 + \mathrm{RnPr}}\right),\quad f_6 = \left(\frac{M^2 \mathrm{Br}}{1 + \mathrm{RnPr}}\right),\quad f_7 = \frac{f_6 f_3^2}{16\, r_1^2},\quad f_8 = \frac{f_6 f_4^2}{16\, r_2^2},$$

$$f_9 = \frac{f_6 f_3 f_4}{2(r_1 + r_2)^2},\quad f_{10} = \frac{f_6 f_3 f_4}{2(r_1 - r_2)^2},\quad f_{11} = \frac{f_2 f_3}{r_1^2},\quad f_{12} = \frac{f_2 f_3}{r_2^2},$$

$$f_{13} = \left(\frac{f_3^2}{2} + \frac{f_4^2}{2} + f_2^2\right),\quad f_{14} = (f_5 - f_{13}),\quad f_{15} = 4f_7 r_1,$$

$$f_{16} = 4f_8 r_2,\ f_{17} = 2f_9(r_1 + r_2),\ f_{18} = 2f_{10}(r_1 - r_2),\ f_{19} = 2f_{11} r_1,$$

$$f_{20} = 2f_{12} r_2,$$

$$\begin{aligned}f_{21} = {} & (f_5 - f_{13})\frac{h^2}{2} - 2f_7 \cosh[2r_1 h] - 2f_8 \cosh[2r_2 h], \\ & - 2f_9 \cosh[(r_1 + r_2)h] - 2f_{10}\cosh[(r_1 - r_2)h] \\ & - 2f_{11}\cosh[r_1 h] + 2f_{12}\cosh[r_2 h]\end{aligned}$$

$$\begin{aligned}f_{22} = {} & f_{14}\ \mathrm{h} - f_{15}\sinh[2r_1 h] - f_{16}\sinh[2r_2 h] - f_{17}\sinh[(r_1 + r_2)h] \\ & - f_{18}\sinh[(r_1 - r_2)h] - f_{19}\sinh[r_1 h] + f_{20}\sinh[r_2 h],\end{aligned}$$

$$f_{23} = -f_{21} - \beta_1 f_{22}.$$

Now,

$$\begin{aligned}\Phi(y) = {} & f_{40}\cosh[r_3 y] - f_{31} - f_{32}\cosh[2r_1 y] \\ & - f_{33}\cosh[2r_2 y] - f_{34}\cosh[(r_1 + r_2)y] \\ & - f_{35}\cosh[(r_1 - r_2)y] - f_{36}\cosh[r_1 y] \\ & + f_{37}\cosh[r_2 y],\end{aligned} \tag{25}$$

where

$$f_{24} = \mathrm{Sc}\ \mathrm{Sr},\ f_{25} = (2f_{15} r_1),\ f_{26} = (2f_{16} r_2),\ f_{27} = f_{17}(r_1 + r_2),$$

$$f_{28} = f_{18}(r_1 - r_2),\quad f_{29} = f_{19} r_1,\quad f_{30} = f_{20} r_2,\quad f_{31} = \left(\frac{f_{14} f_{24}}{b}\right),$$

$$f_{32} = \frac{f_{24} f_{25}}{4r_1^2 - b},\quad f_{33} = \frac{f_{24} f_{26}}{4r_2^2 - b},\quad f_{34} = \frac{f_{24} f_{27}}{(r_1 + r_2)^2 - b},\quad f_{35} = \frac{f_{24} f_{28}}{(r_1 - r_2)^2 - b},$$

$$f_{36} = \frac{f_{24} f_{29}}{r_1^2 - b},\ f_{37} = \frac{f_{24} f_{30}}{r_2^2 - b},\ r_3 = \sqrt{S\ \mathrm{Sc}},\ b = S\ \mathrm{Sc},$$

$$\begin{aligned}f_{38} = {} & -f_{31} - f_{32}\cosh[2r_1 h] - f_{33}\cosh[2r_2 h] \\ & - f_{34}\cosh[(r_1 + r_2)h] - f_{35}\cosh[(r_1 - r_2)h] \\ & - f_{36}\cosh[r_1 h] + f_{37}\cosh[r_2 h]\end{aligned}$$

$$\begin{aligned}f_{39} = {} & -2r_1 f_{32}\cosh[2r_1 h] - 2r_2 f_{33}\cosh[2r_2 h] - (r_1 + r_2) f_{34}\cosh[(r_1 + r_2)h]. \\ & - (r_1 - r_2) f_{35}\cosh[(r_1 - r_2)h] - r_1 f_{36}\cosh[r_1 h] + r_2 f_{37}\cosh[r_2 h]\end{aligned}$$

The rate of volumetric flow is referred to as:

$$\begin{aligned}q = {} & \int_0^h u\,dy = \int_0^h (f_3 \cosh[r_1 y] + f_4 \cosh[r_2 y] - f_2)\,dy \\ & = f_{41}\sinh[r_1 h] + f_{42}\sinh[r_2 h] - f_{40} h - \frac{1}{f_1}\left(\left(\frac{dp}{dx}\right)h\right),\end{aligned} \tag{26}$$

where

$$f_{40} = \frac{1}{f_1}\left(M^2 + \frac{1}{\mathrm{Da}} - \eta_1 \sin\gamma\right),\ f_{41} = \frac{f_3}{r_1},\ \text{and}\ f_{42} = \frac{f_4}{r_2}.$$

From Eq. (26), the pressure gradient $\left(\frac{dp}{dx}\right)$ is expressed as:

$$\frac{dp}{dx} = \frac{1}{h}(q f_1 - f_{43}\sinh[r_1 h] - f_{44}\sinh[r_2 h] + f_{45} h), \tag{27}$$

where

$$f_{43} = (f_1 f_{41}),\ f_{44} = (f_1 f_{42}),\ \text{and}\ f_{45} = (f_1 f_{40}).$$

The instantaneous flux $Q(x, t)$ equals

$$Q(x,\ t) = \int_0^h (u + 1)dy = q + h. \tag{28}$$

The average volume flow rate is often indicated as:

$$\bar{Q} = \frac{1}{T}\int_0^T Q dt = q + 1. \tag{29}$$

The pressure gradient can be mathematically represented using Eqs. (27) and (29):

$$\frac{dp}{dx} = \frac{1}{h}\left((\bar{Q} - 1)f_1 - f_{43}\sinh[r_1 h] - f_{44}\sinh[r_2 h] + f_{45}h \right). \tag{30}$$

According to reference [62], the skin friction coefficient (C_f), the Nusselt number (Nu), and the Sherwood number (Sh) are used to define shear stress, heat transfer rate, and mass transfer rate, respectively, at the wall:

$$C_f = h_x u'(h),\ \mathrm{Nu} = h_x \theta'(h),\ \mathrm{Sh} = h_x \Phi'(h). \tag{31}$$

4 Discussion of the problem

In this section, we examine the effects of various emergent components on the distributions of velocity, skin friction, temperature, and concentration. These are the default settings for the parameters used in calculations: $\varepsilon = 0.2$, $\phi = \frac{\pi}{3}$, $x = 0.5$, $t = 0.2$, $d = 0.1$, $\rho = 0.1$, $\mu = 0.1$, $\eta_1 = 0.5$, $p = -0.1$, $\alpha = 10$, $\gamma = \frac{\pi}{2}$, $\mathrm{Da} = 0.2$, $M = 2.5$, $\mathrm{Br} = 0.5$, $\mathrm{Rn} = 0.5$, $\mathrm{Pr} = 2.5$, $\beta = 0.5$, $\Omega = 10$, $\beta_1 = 0.5$, $\beta_2 = 0.3$, $\mathrm{Sr} = 1.5$, $\mathrm{Sc} = 0.1$, and $S = 0.2$. For numerical analysis, we resort to the Mathematica software.

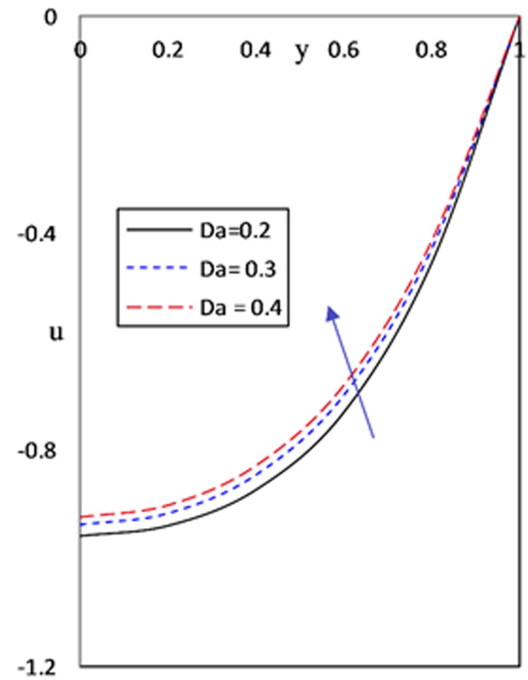

Figure 3: Significance of porosity parameter on velocity (u).

4.1 Velocity distribution

The fluid velocity as a function of y is illustrated in Figures 2–6. Figure 2 conveys the consequence of the Hartmann number (M) on u. The velocity profile is seen to decrease

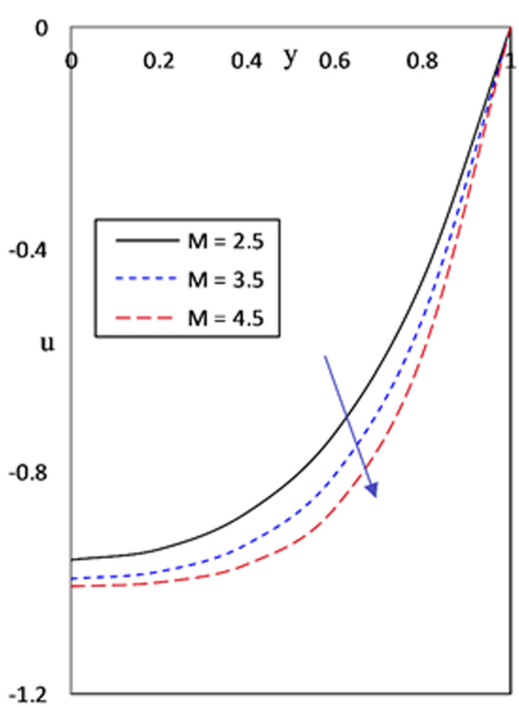

Figure 2: Significance of Hartmann on velocity (u).

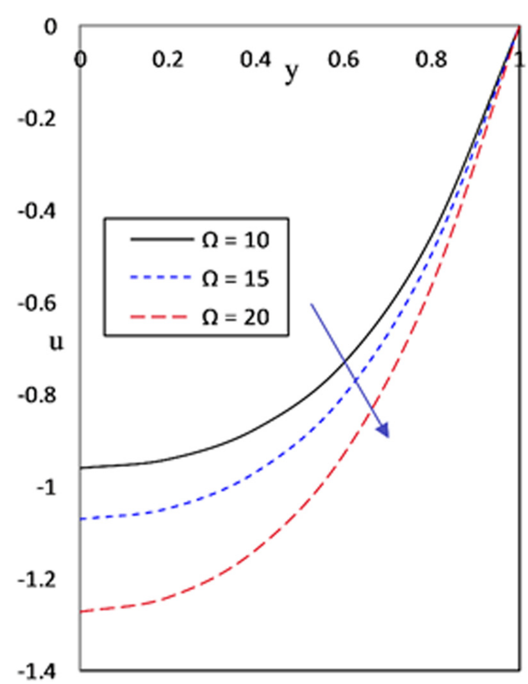

Figure 4: Significance of rotation on velocity (u).

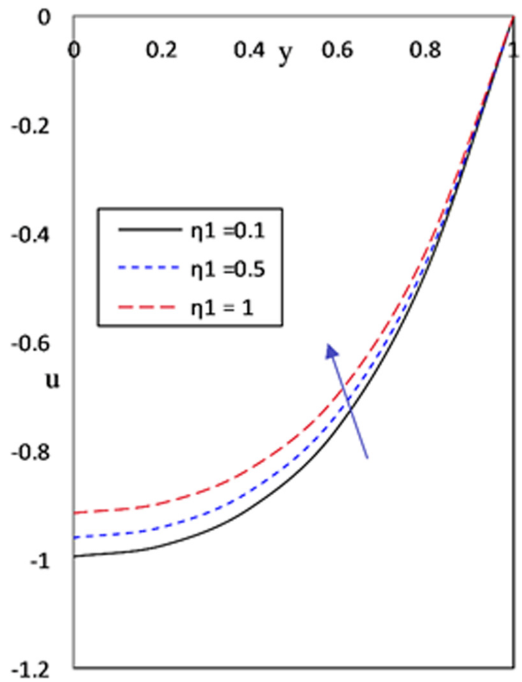

Figure 5: Significance of gravitational parameter on velocity (u).

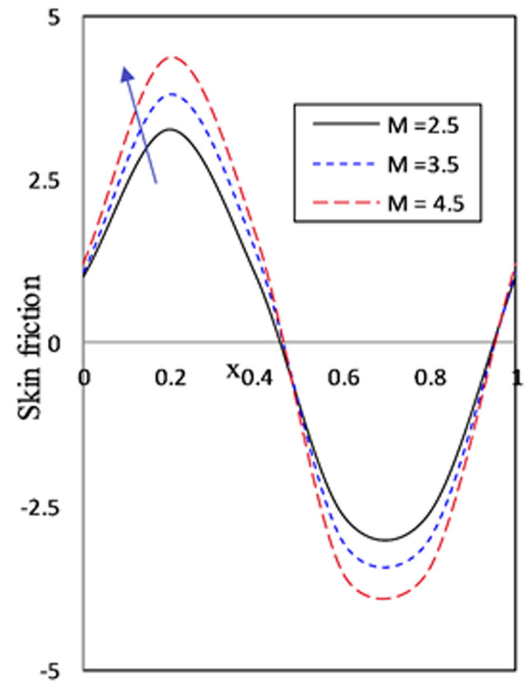

Figure 7: Significance of Hartmann on skin friction (C_f).

with increasing M. This is brought on by Lorentz forces' retarding effect on the velocity of the fluid. The relationship between Da and fluid velocity is seen in Figure 3. Increasing the porosity parameter results in a higher fluid velocity. Physically, fluid flow is enabled by a porous medium with high permeability. Figure 4 displays the change in fluid velocity as a function of Ω. The absolute velocity of the fluid drops as Ω increases. Figures 5 and 6 show that the velocity of the fluid increases when the gravitational and couple stress parameters are both increased.

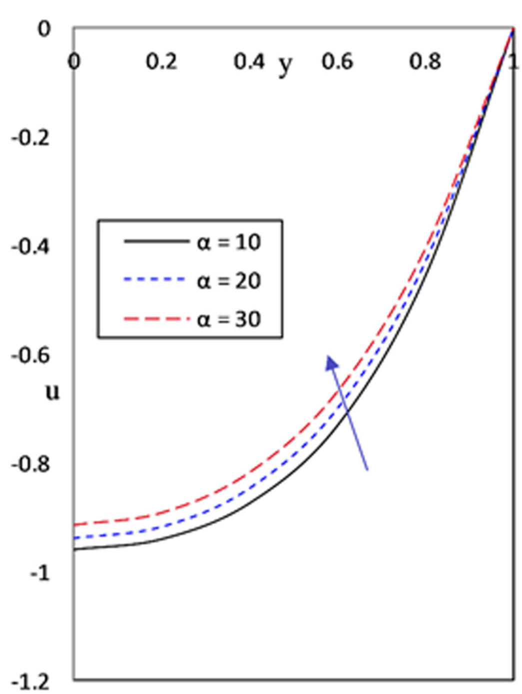

Figure 6: Significance of couple stress parameter on velocity (u).

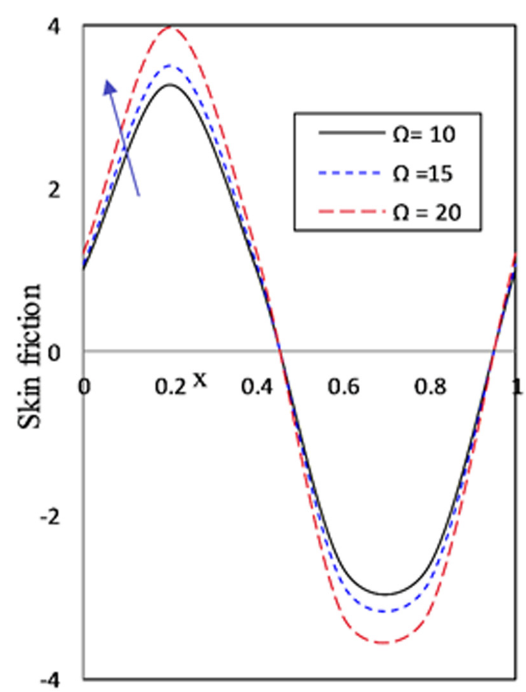

Figure 8: Significance of rotation on skin friction (C_f).

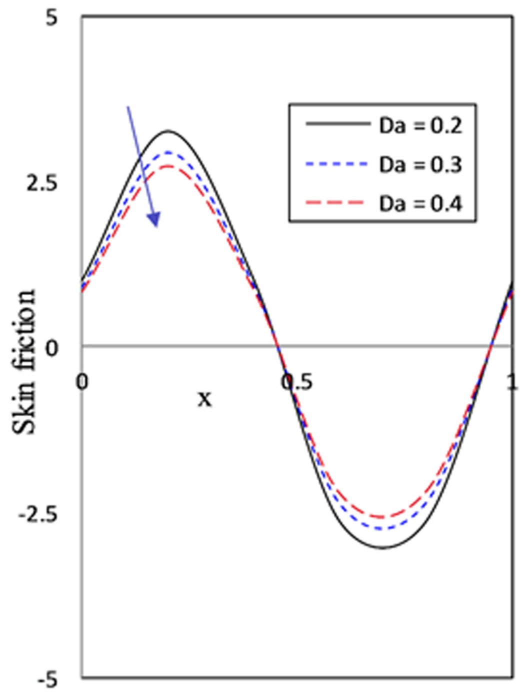

Figure 9: Significance of porosity parameter on skin friction (C_f).

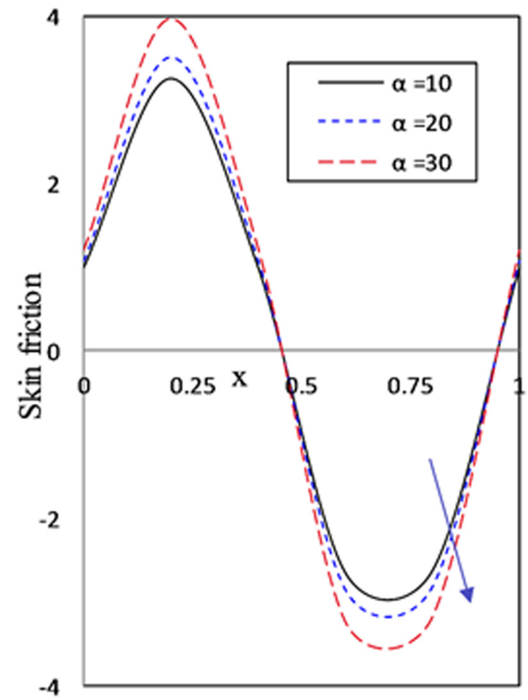

Figure 11: Significance of couple stress parameter on skin friction (C_f).

4.2 Skin friction

Figures 7–11 show the results of varying M, Da, Ω, η_1, and α to demonstrate how they affect the skin friction coefficient C_f. The observed trend in Figures 7 and 8 indicates that an increase in both M and Ω leads to a rise in the skin friction coefficient inside the region $x \in (0, 0.5)$, whereas a drop is seen in the other section of the channel, $x \in (0.5, 1)$. The C_f as affected by Da is seen in Figure 9. The aforementioned graph shows that the C_f decreases between $x = 0$ and $x = 0.5$, while it improves between

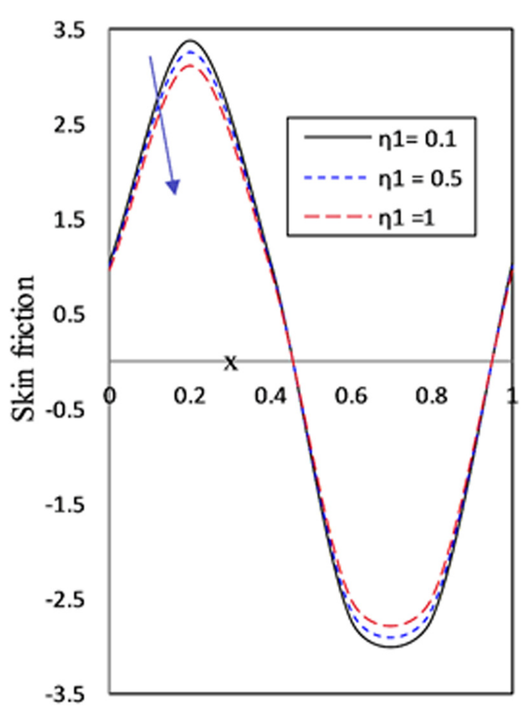

Figure 10: Significance of gravitational parameter on skin friction (C_f).

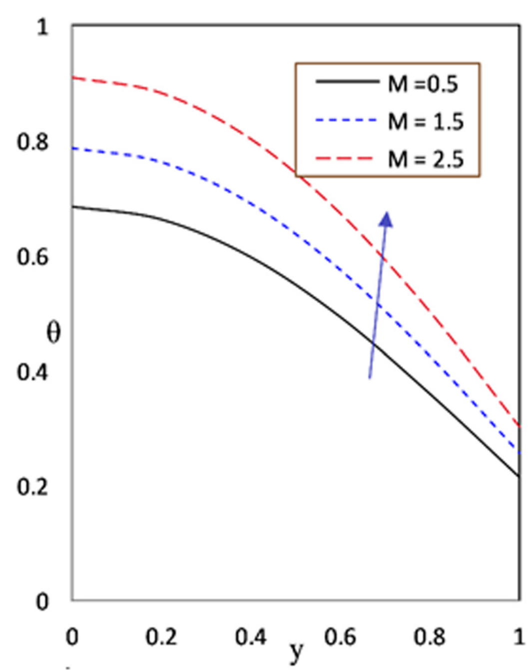

Figure 12: Significance of Hartmann on temperature (θ).

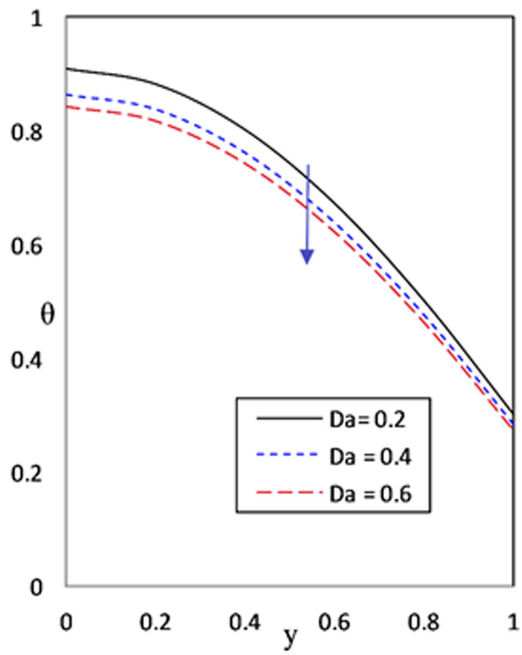

Figure 13: Significance of porosity parameter on temperature (θ).

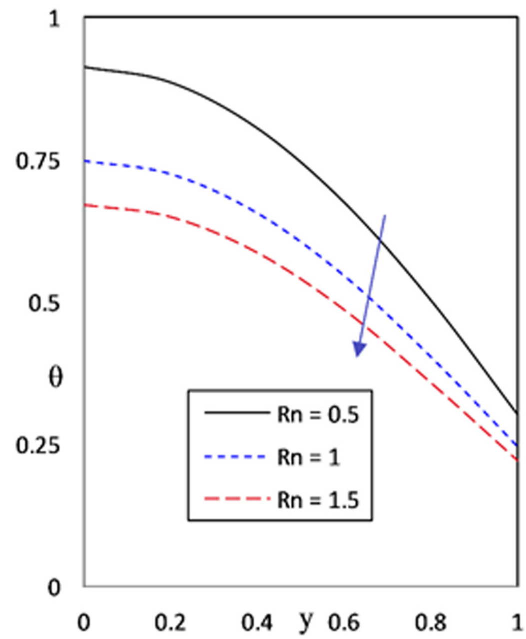

Figure 15: Significance of thermal radiation on temperature (θ).

$x = 0.5$ and $x = 1$. In Figure 10, the influence of η_1 on C_f is presented. In the area of the channel between $x = 0$ and $x = 0.5$, the skin friction coefficient decreases as η_1 rises. However, the skin friction coefficient measurements are unremarkable along the sides of the channel. From Figure 11, as α is increased, we see that the skin friction coefficient improves in the range of $x = 0$ to $x = 0.5$.

4.3 Heat transfer analysis

Figures 12–19 exhibit the temperature pattern (θ or $\theta(y)$) as a function of y for different values of the parameters. Figure 12 demonstrates that as M increases, so does the temperature of the fluid. The force of Lorentz, which

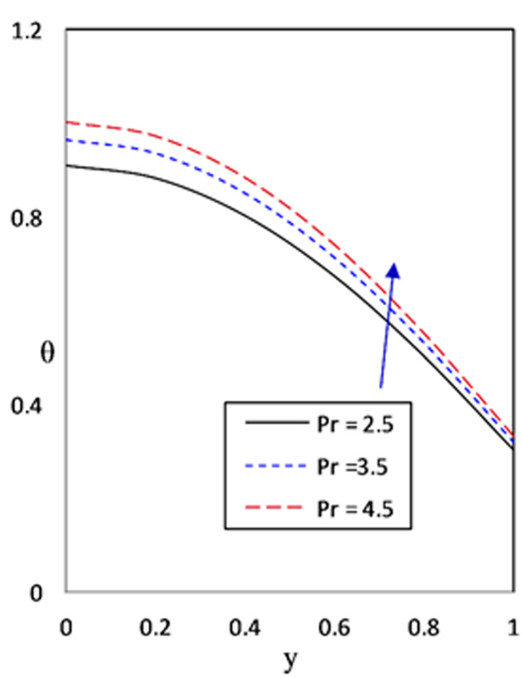

Figure 14: Significance of Prandtl number on temperature (θ).

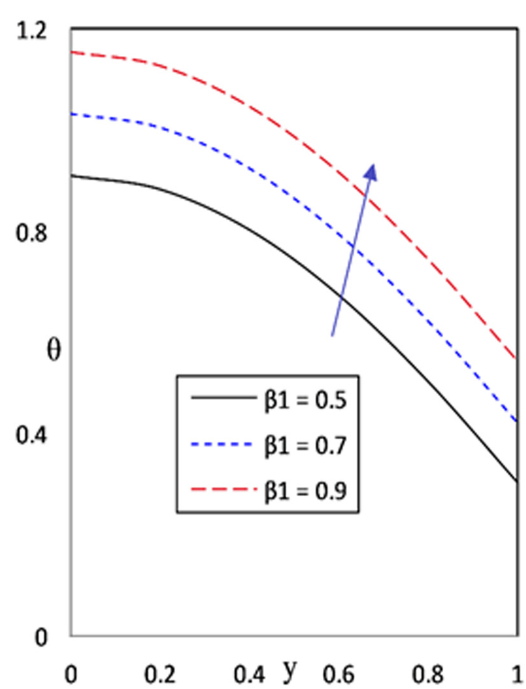

Figure 16: Significance of thermal slip parameter on temperature (θ).

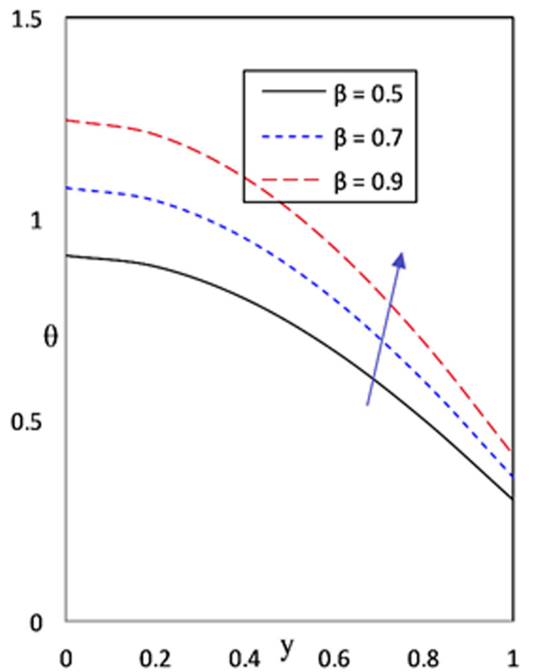

Figure 17: Significance of heat source parameter on temperature (θ).

opposes the motion of the fluid, causes an increase in the resistance of the fluid to motion, which in turn causes an increase in the temperature of fluid. Figure 13 shows how Da affects the temperature profile. This graph shows that when Da increases, the fluid temperature drops because the boundary layer becomes thicker. Figure 14 shows the

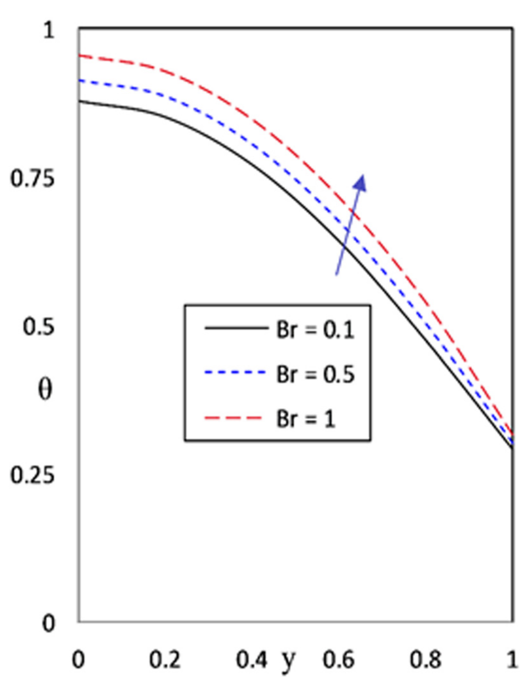

Figure 18: Significance of Brinkman number on temperature (θ).

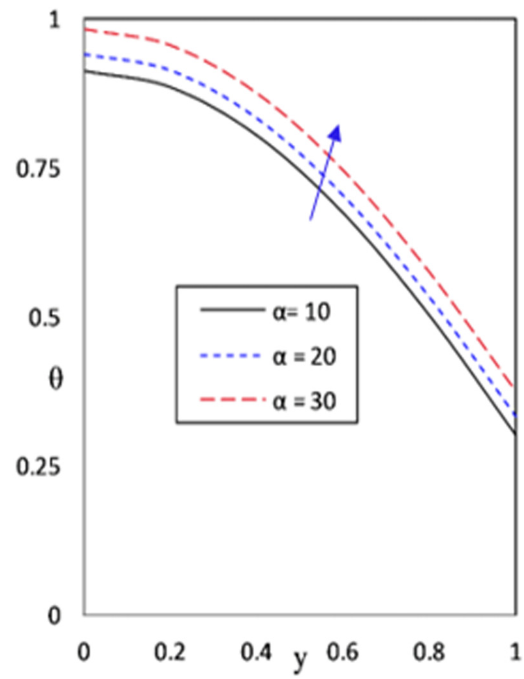

Figure 19: Significance of couple stress parameter on temperature (θ).

temperature variation as a function of the Prandtl number. As Pr rises, so does the temperature of fluid. A rise in the Prandtl number results in a magnification of the interfacial shear stress between adjacent layers of the fluid. Consequently, an increased Pr value indicates an increased temperature. Figure 15 depicts the influence of Rn on $\theta(y)$. In reality, when the thermal radiation parameter rises, the fluid temperature falls. The fluid temperature increases with increasing β_1, as seen in Figure 16. As the slip parameter (β_1) enhances, the temperature profile rises because

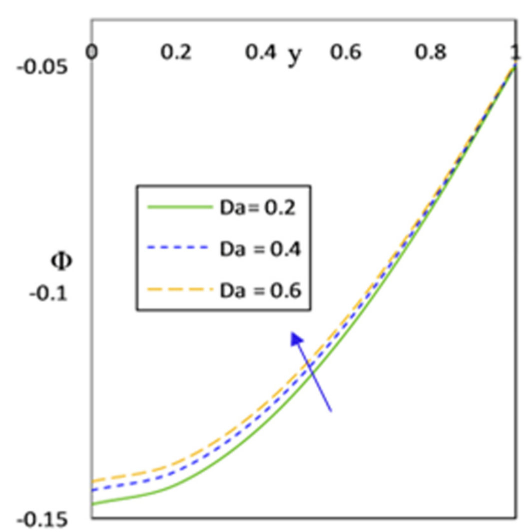

Figure 20: Significance of porosity parameter on concentration (Φ).

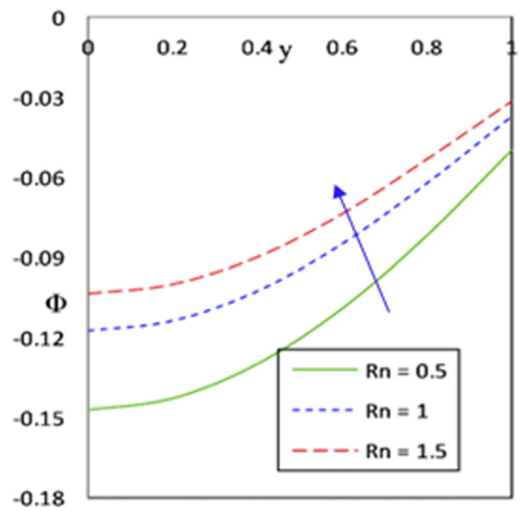

Figure 21: Significance of thermal radiation on concentration (Φ).

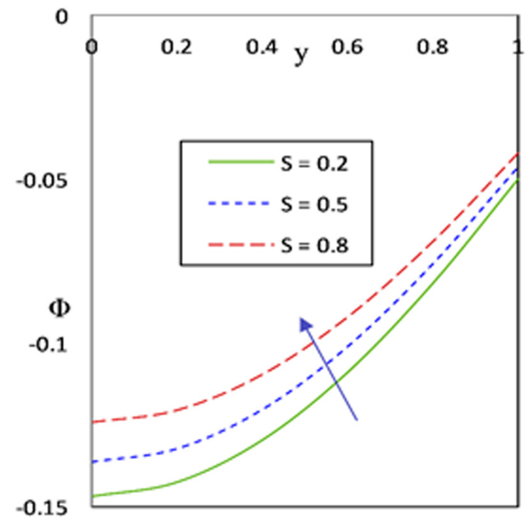

Figure 22: Significance of chemical reaction parameter on concentration (Φ).

more heat is transmitted from the surface to the liquid. The temperature distribution with β is shown in Figure 17. A rise in the heat source/sink parameter results in higher-temperature profiles because the thermal boundary layer is thinner. The impact of Br on $\theta(y)$ is seen in Figure 18. Since the Brinkman number is proportional to the amount of viscous dissipation, it can be shown that it has a major impact on the flow and that more accurate Brinkman number estimates lead to a more desirable temperature profile. Figure 19 illustrates the fluctuation in temperature profile in response to different values of α. The graph elucidates that the progressive increments in the values of α result in an increase in the temperature profile.

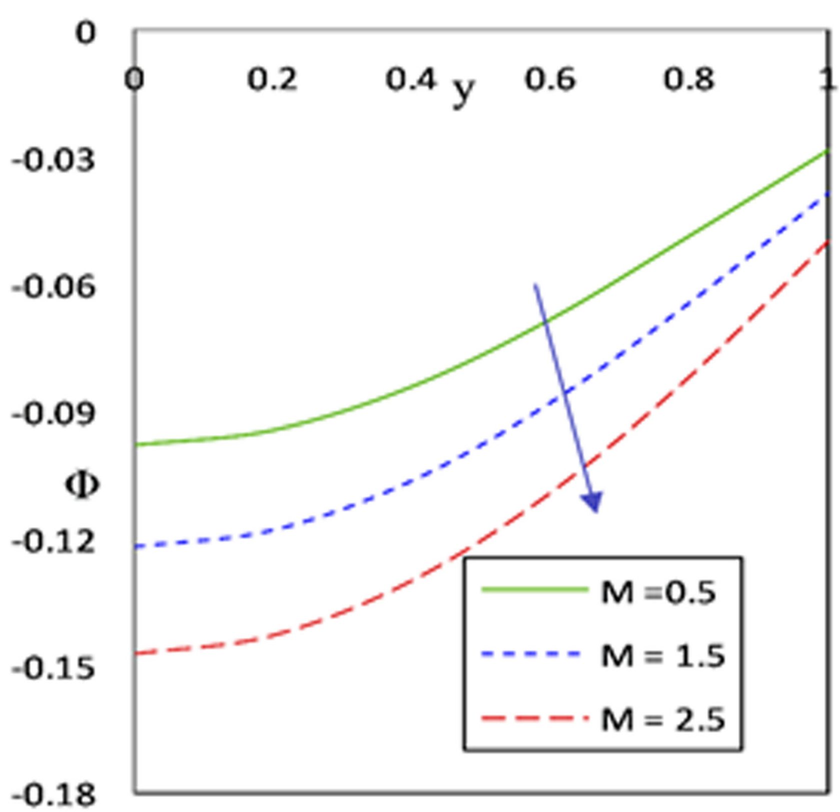

Figure 23: Significance of Hartmann number on concentration (Φ).

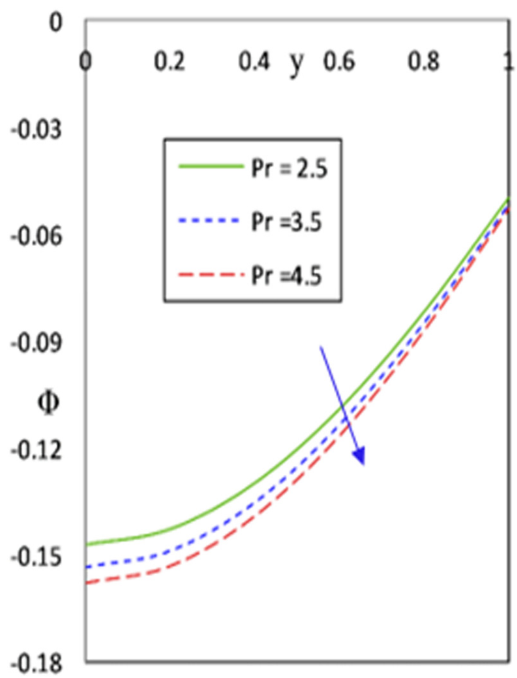

Figure 24: Significance of Prandtl number on concentration (Φ).

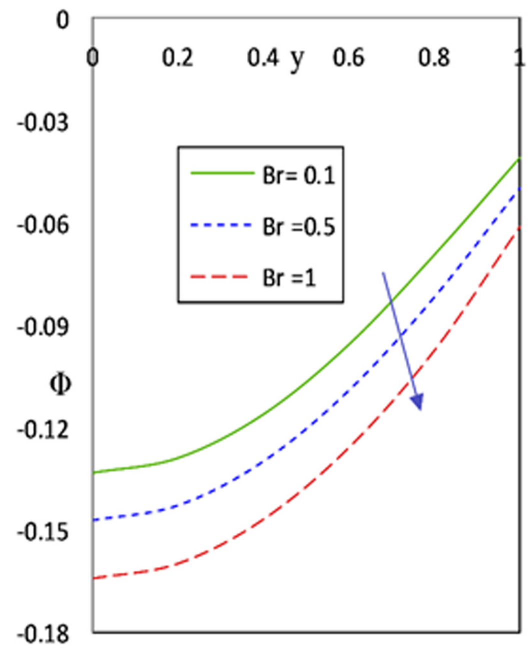

Figure 26: Significance of Brinkman number on concentration (Φ).

4.4 Mass transfer analysis

There are provided graphical representations 20–29 of how diverse factors influence the concentration profile (Φ or $\Phi(y)$). Figures 20 and 21 depict the role of Da and Rn on the distribution of concentration. These charts show that a rise in Da and Rn results in a corresponding increase in fluid concentration. As depicted in Figure 22, the fluid concentration improves as the chemical reaction parameter increases. Concentration distribution changes caused by M, Pr, α, Br, β_2, Sr, and Sc are shown in

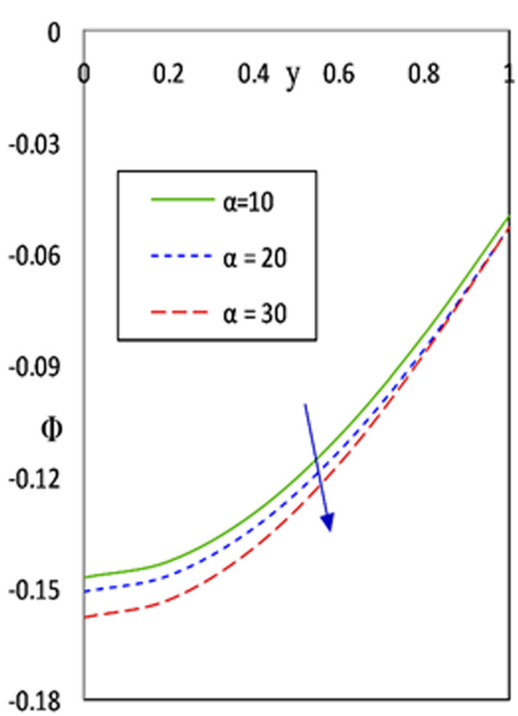

Figure 25: Significance of couple stress parameter on concentration (Φ).

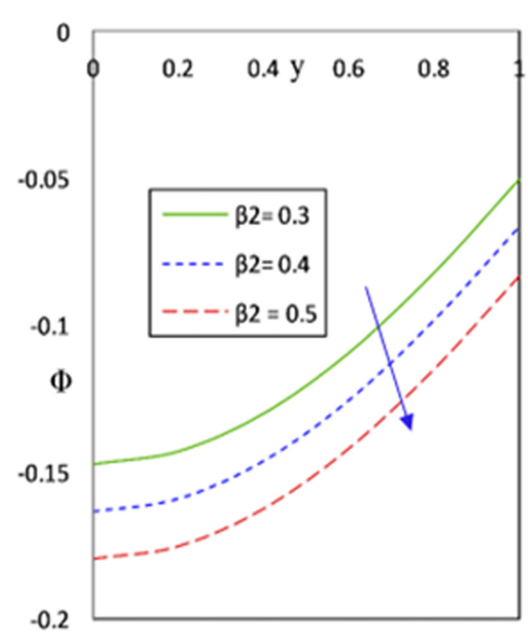

Figure 27: Significance of concentration slip parameter on concentration (Φ).

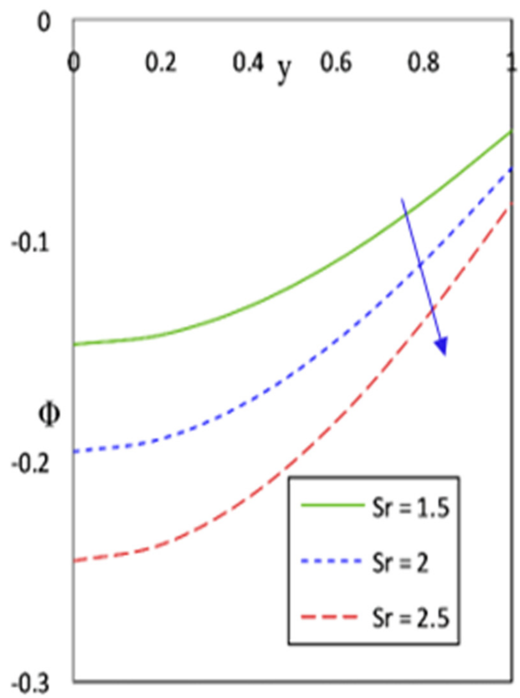

Figure 28: Significance of Soret number on concentration (Φ).

Figure 23 through 29. The graphs demonstrate that the fluid concentration falls as the values of M, Pr, α, Br, β_2, Sr, and Sc increase (Figures 24–29).

Tables 1 and 2 show the Nusselt number and Sherwood number at the $y = h$ wall for an assortment of fixed

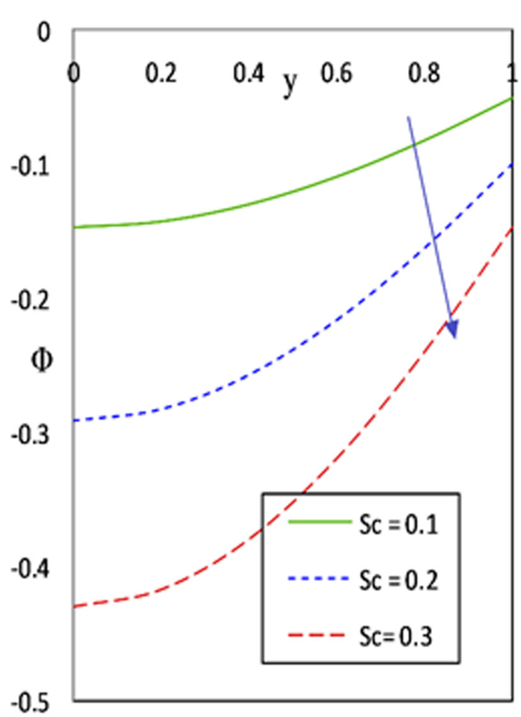

Figure 29: Significance of Schmidt number on concentration (Φ).

Table 1: Nusselt number numerical values at the wall $y = h$

M	Da	Br	Rn	Pr	β	Ω	α	Nusselt number (Nu)
0.5	0.2	0.5	0.5	2.5	0.5	10	10	0.371857
1.5								0.432244
2.5								0.5128
2.5	0.2							0.5128
	0.3							0.505677
	0.4							0.500363
	0.2	0.1						0.452018
		0.5						0.5128
		1						0.588778
		0.5	0.5					0.5128
			1					0.393962
			1.5					0.33767
			0.1	2.5				0.5128
				3.5				0.536334
				4.5				0.552627
				2.5	0.5			0.5128
					0.7			0.615508
					0.8			0.718216
					0.5	10		0.5128
						15		0.515326
						20		0.516794
						10	10	0.5128
							20	0.541496
							30	0.543337

values of $\varepsilon = 0.2$, $\phi = \frac{\pi}{3}$, $x = 0.5$, $t = 0.2$, and $\eta_1 = 0.5$ respectively. Nusselt and Sherwood values demonstrate the efficacy of surface heat and mass convection. Sherwood number for the concentration boundary layer is comparable to the Nusselt number for the thermal boundary layer. According to Table 1, an increase in M, Br, Pr, β, Ω, and α causes the Nusselt number to increase, whereas an increase in Da and Rn causes the Nusselt number to lessen. Sherwood number results decrease with increasing M, Br, Pr, β, Ω, Sc, and Sr, but increase with increasing Da, Rn, and S, as shown in Table 2.

5 Conclusions

Examining the peristalsis process in the flow of a pair stress fluid through an inclined channel with a porous material present is the focus of this study. The study takes into account not only the role of reaction mechanism and Ohmic heating, but also slip boundary conditions. The most significant results are referenced as follows:

1) The fluid flow of velocity enhances with a rise in Da, η_1, and α, whereas it decelerates with an increase in Ω and M.
2) The skin friction coefficient rises in the channel region $x = 0$ to $x = 0.5$, whereas it decelerates in the other

Table 2: Sherwood number numerical values at the wall $y = h$

M	Da	Br	Rn	Pr	β	Ω	S	Sc	Sr	Sherwood number (Sh)
0.5	0.2	0.5	0.5	2.5	0.5	10	0.2	0.1	1.5	−0.0534638
1.5										−0.0673244
2.5										−0.0821678
2.5	0.2									−0.0821678
	0.3									−0.0814932
	0.4									−0.0809408
	0.2	0.1								−0.070517
		0.5								−0.0821678
		1								−0.0967312
		0.5	0.5							−0.0821678
			1							−0.0634352
			1.5							−0.0545619
			0.1	2.5						−0.0821678
				3.5						−0.0850308
				4.5						−0.0870129
				2.5	0.5					−0.0821678
					0.7					−0.0973229
					0.8					−0.112478
						10				−0.0821678
						15				−0.0941432
						20				−0.120531
						10	0.2			−0.0821678
							0.5			−0.0800682
							0.8			−0.0780732
							0.2	0.1		−0.0821678
								0.2		−0.161512
								0.3		−0.238176
								0.1	1.5	−0.0821678
									2	−0.109557
									2.5	−0.136946

part of the portion $x = 0.5$ *to* $x = 1$ with an increase in M and Ω, while the trend is reverse in case of Da and η_1.

3) The fluid temperature reduces with a rise in Da and Rn, while it improves with a rise in M, Pr, β_1, β, Br, and α.
4) The fluid concentration decelerates as the values of M, Pr, α, Br, β_2, Sr, and Sc increase.
5) An increase in M, Br, Pr, β, Ω, and α causes the Nusselt number to improve, whereas an increase in Da and Rn causes the Nusselt number to lessen.
6) Sherwood number results decrease with increasing M, Br, Pr, β, Ω Sc, and Sr but increase with increasing Da, Rn, and S.

Several aspects of human physiology may be profoundly affected by the findings of this study. Porosity is frequently observed in a substantial proportion of human organs. Consequently, the mathematical model presented in this study can be used to predict the effectiveness of various systems. Incorporating nanoparticles, nanoparticle hybrids, and viscous dissipation into a comprehensive mathematical framework has the potential to advance research into cancer treatment strategies in physiological systems. Incorporating Dufour effects and convective boundary conditions is one possible methodology for developing a thermal analysis model of the digestive system. The aforementioned research demonstrates the diversity of possible applications for peristalsis in a variety of disciplines of study.

Acknowledgments: The authors acknowlegde Researchers Supporting Project number (RSPD2023R576), King Saud University, Riyadh, Saudi Arabia.

Funding information: Researchers Supporting Project number (RSPD2023R576), King Saud University, Riyadh, Saudi Arabia.

Author contributions: All authors have accepted responsibility for the entire content of this manuscript and approved its submission.

Conflict of interest: The authors state no conflict of interest.

Data availability statement: The datasets generated and/or analysed during the current study are available from the corresponding author on reasonable request.

References

[1] Eldabe NT, Hassan MA, Abou-Zeid MY. Wall properties effect on the peristaltic motion of a coupled stress fluid with heat and mass transfer through a porous medium. J Eng Mech. 2016;142:04015102.
[2] Abou-Zeid MY. Homotopy perturbation method for couple stresses effect on MHD peristaltic flow of a non-Newtonian nanofluid. Microsyst Technol. 2018;24:4839–46.
[3] Alsaedi A, Ali N, Tripathi D, Hayat T. Peristaltic flow of couple stress fluid through uniform porous medium. Appl Math Mech. 2014;35:469–80.
[4] Ravikumar S, Siva Prasad R. Interaction of Pulsatile flow on the peristaltic motion of couple stress fluid through Porous medium in a flexible channel. Eur J Pure Appl Math. 2010;3:213–26.
[5] Ravikumar S. Effect of couple stress fluid flow on magnetohydrodynamic peristaltic blood flow with porous medium through inclined channel in the presence of slip effect - blood flow model. Int J Biosci Biotechnol. 2015;7:65–84.
[6] Ravikumar S. The effect of the couple stress fluid flow on MHD peristaltic motion with uniform porous medium in the presence of slip effect. Jordan J Mech Ind Eng. 2015;9:269–78.
[7] Abbas Z, Shakeel A, Rafiq M, Khaliq S, Hasnain J, Nadeem A. Rheology of peristaltic flow in couple stress fluid in an inclined tube: Heat and mass transfer analysis. Adv Mech Eng. 2022;14:1–14.
[8] Ismael AM, Eldabe NT, Abou Zeid MY. Thermal micropolar and couple stresses effects on peristaltic flow of bi-viscosity nanofluid through a porous medium. Sci Rep. 2022;12:16180.

[9] Vaidya H, Rajashekhar C, Manjunatha G, Prasad KV, Makinde OD, Vajravelu K. Heat and mass transfer analysis of MHD peristaltic flow through a complaint porous channel with variable thermal conductivity. Phys Scr. 2020;95:1–11.

[10] Rafiq MY, Abbas Z, Ullah MZ. Peristaltic mechanism of couple stress nanomaterial in a tapered channel. Ain Shams Eng J. 2022;13:1–11.

[11] Hayat T, Asghar S, Tanveer A, Alsaedi A. Chemical reaction in peristaltic motion of MHD couple stress fluid in channel with Soret and Dufour effects. Res Phys. 2018;10:69–80.

[12] Ellahi R, Zeeshan A, Hussain F, Asadollahi A. Peristaltic blood flow of couple stress fluid suspended with nanoparticles under the influence of chemical reaction and activation energy. Symmetry. 2019;11:2–17.

[13] Ramachandraiah V, Nagaradhika V, Sivaprasad R, Subba Rao A, Rajendra P. MHD effects on peristaltic flow of a couple stress fluid in a channel with permeable walls. Int J Math Trends Technol. 2018;58:24–37.

[14] Sankad GC, Nagathan PS. Transport of MHD couple stress fluid through peristalsis in a porous medium under the influence of heat transfer and slip effects. Int J Appl Mech Eng. 2017;22:403–14.

[15] Latham TW. Fluid motion in a peristaltic pump. M S. Thesis. Cambridge, M.A: Massachusetts Institute of Technology; 1966.

[16] Shapiro AH, Jaffrin MY, Wienberg SL. Peristaltic pumping with long wavelengths at low Reynolds number. J Fluid Mech. 1969;37:799–825.

[17] Shrinivasacharya D, Mishra M, Rao AR. Peristaltic pumping of a Micropolar fluid in a tube. Acta Mech. 2003;161:165–78.

[18] Vajravelu K, Radhakrishnamacharya G, Radhakrishnmurthy V. Peristaltic flow and heat transfer in a vertical porous annulus with long wave approximation. Int J Non-Linear Mech. 2007;42:754–9.

[19] Ravikumar S, Khan MI, Reddappa B. The effects of diffusion on the mechanism of peristaltic flow at slip boundaries when internal Joule heating is present. Heat Transf. 2023;52(7):4578–605.

[20] Ravi Kumar S, Abzal SK. Combined influence of hall currents and joule heating on hemodynamic peristaltic flow with porous medium through a vertical tapered asymmetric channel with radiation. Front Heat Mass Transf. 2017;9:1–9.

[21] Ravikumar S. Analysis of heat transfer on MHD peristaltic blood flow with porous medium through coaxial vertical tapered asymmetric channel with radiation – blood flow study. Int J Biosci Biotechnol. 2016;8:395–408.

[22] Ravi Kumar S. Study of Hall current, radiation and velocity slip on hydromagnetic physiological hemodynamic fluid with porous medium through joule heating and mass transfer in presence of chemical reaction. Int J Heat Technol. 2018;36:422–32.

[23] Ravikumar S, Khan MI, Al-Qahtani SA, Eldin SM. Significance of heat and mass transport in peristaltic flow of Jeffrey material subject to chemical reaction and radiation phenomenon through a tapered channel. Open Phys. 2023;21:1–13.

[24] Maiti S, Misra JC. Peristaltic transport of a couple stress fluid: some applications to hemodynamics. J Mech Med Biol. 2012;12(3):1250048. doi: 10.1142/S0219519411004733.

[25] Ravikumar S. Hydromagnetic peristaltic transportation with porous medium through coaxial asymmetric vertical tapered channel and Joule heating. App Appl Math: Int J. 2016;11:735–47.

[26] Shit GC, Roy M. Hydromagnetic effect on inclined peristaltic flow of a couple stress fluid. Alex Engin J. 2014;53:949–58.

[27] Ramesh Babu V, Sreenadh S, Srinivas ANS. Peristaltic transport of a viscous fluid in a porous channel with suction and injection. Ain Shams Eng J. 2018;9:909–15.

[28] Aman S, Al-Mdallal Q, Khan MI. Heat transfer and second order slip effect on MHD flow of fractional Maxwell fluid in a porous medium. J King Saud Univ Sci. 2020;32:450–8.

[29] Hayat T, Farooq S, Ahmad B, Alsaedi A. Characteristics of convective heat transfer in the MHD peristalsis of Carreau fluid with Joule heating. AIP Adv. 2016;6:045302.

[30] Abbasi FM, Hayat T, Alsaedi A. Effects of inclined magnetic field and Joule heating in mixed convective peristaltic transport of non-Newtonian fluids. Bull Pol Acad Sci Tech Sci. 2015;63:501–14.

[31] Hayat T, Rani S, Alsaedi A, Rafiq M. Radiative peristaltic flow of magneto nanofluid in a porous channel with thermal radiation. Res Phys. 2017;7:3396–407.

[32] Prasad KM, Subadra N, Srinivas MAS. Heat and mass transfer effects of peristaltic transport of a nanofluid in peripheral layer. AAM: Int J. 2017;12:968–87.

[33] Bestman AR. Natural convection boundary layer with suction and mass transfer in a porous medium. Int J Energy Res. 1990;14:389–96.

[34] Reddy AMR, Ramana Reddy JV, Sandeep N, Sugunamma V. Effect of nonlinear thermal radiation on MHD chemically reacting Maxwell fluid flow past a linearly stretching sheet studied. AAM: Int J. 2017;12:259–74.

[35] Shah NA, Animasaun IL, Chung JD, Wakif A, Alao FI, Raju CS. Significance of nanoparticle's radius, heat flux due to concentration gradient, and mass flux due to temperature gradient: The case of Water conveying copper nanoparticles. Sci Rep. 2021;11:1882.

[36] Sowmya G, Gireesha BJ, Animasaun IL, Shah NA. Significance of buoyancy and Lorentz forces on water-conveying iron (III) oxide and silver nanoparticles in a rectangular cavity mounted with two heated fins: heat transfer analysis. J Therm Anal Calorim. 2021;144:2369–84.

[37] Punith Gowda RJ, Naveen Kumar R, Jyothi AM, Prasannakumara BC, Nisar KS. KKL correlation for simulation of nanofluid flow over a stretching sheet considering magnetic dipole and chemical reaction. ZAMM J Appl Math Mech/ Z Angew Math Mech. 2021;101(11):e202000372.

[38] Shi QH, Hamid A, Khan MI, Kumar RN, Gowda RJP, Prasannakumara BC. Numerical study of bio-convection flow of magneto-cross nanofluid containing gyrotactic microorganisms with activation energy. Sci Rep. 2021;11:16030. doi: 10.1038/s41598-021-95587-2.

[39] Varun Kumar RS, Alhadhrami A, Punith Gowda RJ, Kumar RN, Prasannakumara BC. Exploration of Arrhenius activation energy on hybrid nanofluid flow over a curved stretchable surface. Z Angew Math Mech. 2021;101(12):e202100035. doi: 10.1002/zamm.v101.1210.1002/ zamm.202100035.

[40] Khan MI MI, Lashin MMA, Khedher NB, Ahmed B, Khan SU, Oreijah M, et al. Peristaltic phenomenon in an asymmetric channel subject to inclined magnetic force and porous space. Bioengineering. 2022;9(10):588. doi: 10.3390/bioengineering9100588.

[41] Zhang P, Liu Z, Yue X, Wang P, Zhai Y. Water jet impact damage mechanism and dynamic penetration energy absorption of 2A12 aluminum alloy. Vacuum. 2022;206:111532.

[42] Wu Z, Lin B, Fan J, Zhao J, Zhang Q, Li L. Effect of dielectric relaxation of epoxy resin on dielectric loss of medium-frequency transformer. IEEE Trans Dielectr Electr Insulation. 2022;29:1651–8.

[43] Li Z, Wang K, Li W, Yan S, Chen F, Peng S. Analysis of surface pressure pulsation characteristics of centrifugal pump magnetic liquid sealing film. Front Energy Res. 2022;10:937299.

[44] Zheng Y, Liu Y, Guo X, Chen Z, Zhang W, Wang Y, et al. Sulfur-doped g-C3N4/rGO porous nanosheets for highly efficient photocatalytic degradation of refractory contaminants. J Mater Sci Technol. 2020;41:117–26.

[45] Bai B, Zhou R, Cai G, Hu W, Yang G. Coupled thermo-hydro-mechanical mechanism in view of the soil particle rearrangement of granular thermodynamics. Computers Geotech. 2021;137:104272.

[46] Bai B, Rao D, Chang T, Guo Z. A nonlinear attachment-detachment model with adsorption hysteresis for suspension-colloidal transport in porous media. J Hydrol. 2019;578:124080.

[47] Jabeen N, Hussain A, Khan ZU, Khedher NB, Alturki M, Khan MI. Ultrastable and high-performance 3D core-shell NiCo2S4@ Bi2O3 nanorod arrays as anode for LiS batteries. J Energy Storage. 2023;72:108519.

[48] Khan MI, Shah F, Ali F, Alzahrani F. First order chemical reaction response in mixed convective Falkner-Skan Sutterby fluid with Cattaneo-Christov heat and mass flux model. Alex Eng J. 2023;80:559–71.

[49] Jamshed W, Mohd Nasir NAA, Qureshi MA, Shahzad F, Banerjee R, Eid MR, et al. Dynamical irreversible processes analysis of Poiseuille magneto-hybrid nanofluid flow in microchannel: A novel case study. Waves Random Complex Media. 2021;1–23. doi: 10.1080/17455030.2021.1985185.

[50] Shahzad F, Jamshed W, Eid MR, Ibrahim RW, Aslam F, Suzilliana Putri Mohamed Isa S, et al. The effect of pressure gradient on MHD flow of a tri-hybrid Newtonian nanofluid in a circular channel. J Magn Magn Mater. 2023;568:170320.

[51] Sun L, Liang T, Zhang C, Chen J. The rheological performance of shear-thickening fluids based on carbon fiber and silica nanocomposite. Phys Fluids. 2023;35:32002.

[52] Xiang J, Liao J, Zhu Z, Li P, Chen Z, Huang J, et al. Directional fluid spreading on microfluidic chip structured with microwedge array. Phys Fluids. 2023;35:62005.

[53] Chu YM, Nazeer M, Khan MI, Ali W, Zafar Z, Kadry S, et al. Entropy analysis in the Rabinowitsch fluid model through inclined Wavy Channel: Constant and variable properties. Int Commun Heat Mass Transf. 2020;119:104980.

[54] Li S, Raghunath K, Alfaleh A, Ali F, Zaib A, Khan MI, et al. Effects of activation energy and chemical reaction on unsteady MHD dissipative Darcy–Forchheimer squeezed flow of Casson fluid over horizontal channel. Sci Rep. 2023;13:2666.

[55] Song YQ, Khan MI, Qayyum S, Gowda RJP, Kumar RN, Prasannakumara BC, et al. Physical impact of thermo-diffusion and diffusion-thermo on Marangoni convective flow of hybrid nanofluid (MnZiFe2O4–NiZnFe2O4–H2O) with nonlinear heat source/sink and radiative heat flux. Mod Phys Lett B. 2021;35:2141006.

[56] Khan MI, Shah F, Khan SU, Ghaffari A, Chu YM. Heat and mass transfer analysis for bioconvective flow of Eyring Powell nanofluid over a Riga surface with nonlinear thermal features. Numer Methods Partial Differ Equ. 2022;38(4):777–93.

[57] Manzoor N, Qasim I, Khan MI, Ahmed MW, Guedri K, Bafakeeh OT, et al. Antibacterial applications of low-pressure plasma on degradation of multidrug resistant V. cholera. Appl Sci. 2022;12:9737.

[58] Rajesh R, Gowd YR. Impact of Hall current, Joule heating and mass transfer on MHD peristaltic hemodynamic Jeffery fluid with porous medium under the influence of chemical reaction. Chem Eng Trans. 2018;71:997–1002.

[59] Imran N, Javed M, Sohail M, et al. Simultaneous effects of heterogeneous-homogeneous reactions in peristaltic flow comprising thermal radiation: Rabinowitsch fluid model. J Mater Res Technol. 2020;9:3520–9.

[60] Abbas Z, Rafiq MY, Hasnain J, et al. Peristaltic transport of a Casson fluid in a non-uniform inclined tube with Rosseland approximation and wall properties. Arab J Sci Eng. 2021;46:1997–2007.

[61] Jaffrin MY, Shapiro AH. Peristaltic pumping. Annu Rev Fluid Mech. 1971;3:13–37.

[62] Machireddy GR, Kattamreddy VR. Impact of velocity slip and Joule heating on MHD peristaltic flow through a porous medium with chemical reaction. J Nigerian Math Soc. 2016;35:227–44.